Scientific Research Publishing

Open Journal of Geology, 2023, 13, 312-336
https://www.scirp.org/journal/ojg
ISSN Online: 2161-7589
ISSN Print: 2161-7570

Contribution to the Petrographic and Geochemical Study of the Karthala Massif Lavas in the Bangaani Area, Grande Comore, Indian Ocean

Samba Cissokho*, Adinane Ahamada, Abdoulaye Ndiaye, Diomaye Yatte, Papa Malick Ngom

Department of Geology, Faculty of Sciences and Technics, Cheikh Anta Diop University of Dakar (UCAD), Dakar, Senegal
Email: *samba.cissokho@ucad.edu.sn

How to cite this paper: Cissokho, S., Ahamada, A., Ndiaye, A., Yatte, D. and Ngom, P.M. (2023) Contribution to the Petrographic and Geochemical Study of the Karthala Massif Lavas in the Bangaani Area, Grande Comore, Indian Ocean. *Open Journal of Geology*, **13**, 312-336.
https://doi.org/10.4236/ojg.2023.135016

Received: March 23, 2023
Accepted: May 23, 2023
Published: May 26, 2023

Abstract

The Bangaani area is located in the northwestern part of the Karthala Massif on the island of Grande Comore, about 10 km from the capital Moroni. It is essentially constituted of basalt plateaus outcropping in the form of pahoehoe and aa lava flows or in the form of massive vesicular or non vesicular basalt flows. Petrographic analysis of the massive basalts studied shows a porphyritic microlitic texture marked by the successive crystallization of olivines, opaque minerals, clinopyroxenes and plagioclases in a relatively abundant mesostasis. This crystallization sequence is typical of a high pressure environment corresponding to primary alkaline magmas. The geochemical study of major and trace elements shows that the basalts studied are under saturated in silica (47.24%) but rich in alkali (2.26%) and titanium (2.66%). They correspond to intraplate alkaline basalts of type oceanic island basalts (OIB) and present a primary character marked by relatively high contents of magnesium (6.69%), chromium (151.23 ppm), nickel (107.53 ppm) and scandium (27.15 ppm). The REE and multi-element diagrams confirm that the Karthala basalts are alkaline basalts of type OIB by their enrichment in LILE and their depleted character in HREE and HFSE. In terms of isotopic ratios, they are comparable to HIMU and EM I.

Keywords

Bangaani, Karthala, Comore, Alkaline Basalts, OIB

1. Introduction

The Comoros archipelago is located at the northern end of the Mozambique

Channel, halfway between the west coast of Madagascar and the east coast of Africa [1]. It is composed of four islands aligned along an NW-SE axis (**Figure 1**): Grande Comore or Ngazidja in the NW; the islands of Mohéli and Anjouan in the center and the island of Mayotte in the SE [2].

The Grande Comore (**Figure 2**) where our study area is located includes several massifs from a geomorphological point of view: the Grille massif in the north, the Karthala massif in the center and the Badjini massif in the extreme south. On the southern and eastern flanks of the volcano, some areas have a concave morphology and steep slopes [3]. The study area is located in the Karthala massif, which reaches an altitude of 2361 m. It is a basaltic shield volcano constituting alone the two thirds of the island of Grande Comore. It is characterized by the existence of two major rift zones diametrically opposed on either side of a summit caldera resulting from the association of several collapse units [3]. On the southern and eastern flanks of the volcano, some areas have a concave morphology and steep slopes [3].

The Bangaani area is more precisely located (**Figure 3**) between 11˚35'0"S and 11˚36'0"S latitude and 43˚16'0"E and 43˚18'0"E longitude.

The origin of the Comoros Islands is the subject of many controversies related to several geodynamic contexts of setting:

- [2], then [4], put forward the hypothesis of a hot spot based on the dating of basaltic rocks of the archipelago, which seem to indicate islands growing in age from West to East;
- according to [5] in [1], these islands would result from the emergent parts of a slow accretion wrinkle;
- [6], deny age growth from West to East and propose the presence of lithospheric fractures that led to magmatic upwelling.

Our study, based on new petrographic and geochemical data extracted from the article [7], allows completing the helpful database to understand the geology of the big island.

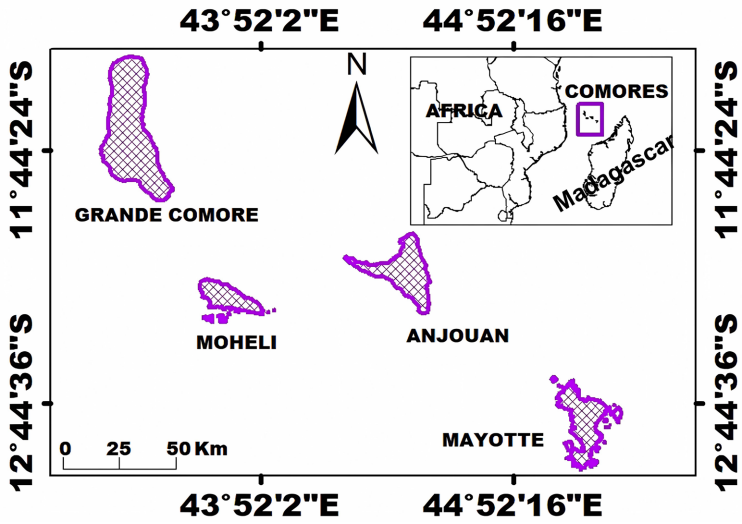

Figure 1. Location map of the Comoros archipelago [2], modified.

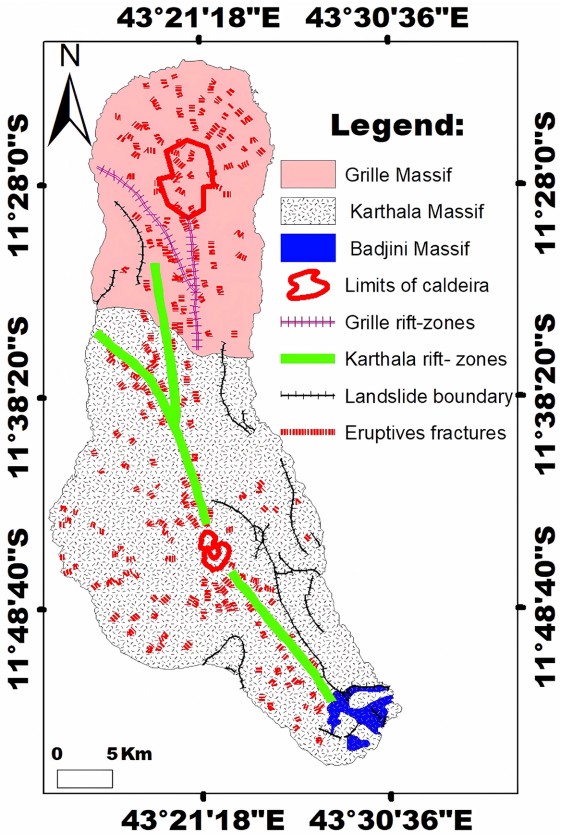

Figure 2. Geomorphological map of Grande Comore [3], modified.

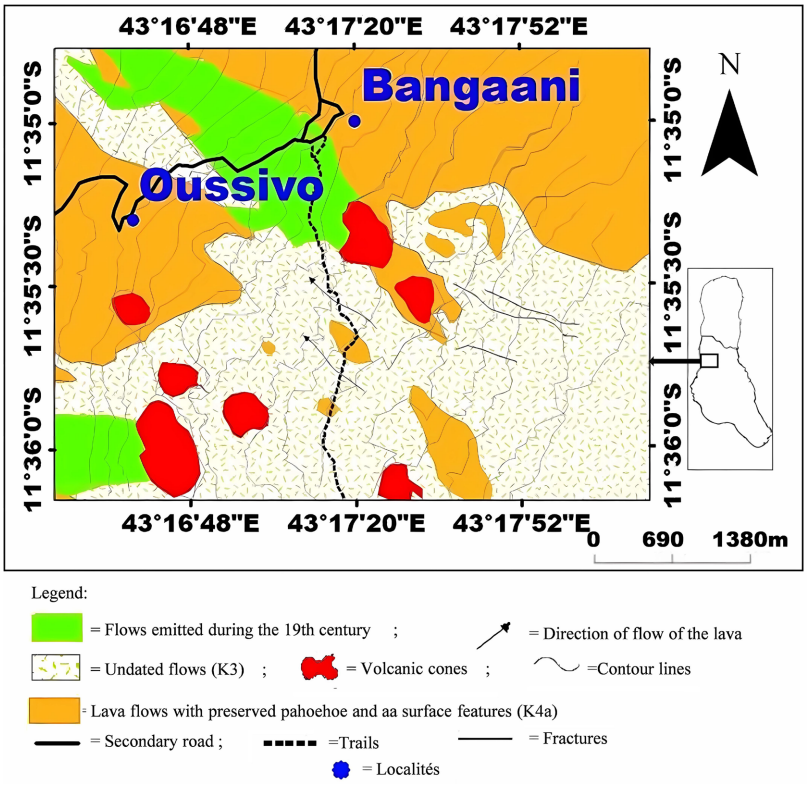

Figure 3. Location map of the Bangaani area [3], modified.

This study's objective is to characterize the Karthala lavas more precisely from a petrographic and geochemical point of view.

2. Regional Geology

The Madagascar block was detached from Africa during the breakup of the Gondwana super continent in the Lower Jurassic [8]. This detachment allowed the construction of the Comoros archipelago in the Cenozoic [9]. These islands were not formed at the same time but as a result of a migration of volcanism during geological time from the east to the west of the archipelago. In the Mio-Pliocene, the oldest island (Maoré) existed about 15MA ago as a large shield volcano [8]. Anjouan and Moheli are therefore of Pliocene age [9]. The building of Grande Comore or Ngazidja, the fourth island, is one of the greatest events of the Quaternary [9].

The formation of the Mozambique Channel is associated with the detachment of the Malagasy microcontinent from Gondwana and took place in several phases [1]:

- karoo rifting associated with a NW-SE trending intracontinental distension phase that occurred from the Permian to the Lower Jurassic and is responsible for the creation of a collapse trough such as the Majunga trough in western Madagascar [10];
- the separation of Madagascar and East Africa is associated with the opening of the Somali and Mozambique basins by oceanic accretion in a N-S direction along the mid-oceanic ridge [1];
- the opening of the Somali and Mozambique oceanic basins from the Middle Jurassic to the Lower Cretaceous by a process of North-South oceanic accretion, associated with a stalling operation of the Davie and Mozambique rifts [1];
- the rotation of Madagascar is linked to the functioning of the Davie chain, more than 1000 km long. This structure delimits a zone of weakness which would have had a dexterous displacement [10] between the Upper Jurassic and the Aptian.

3. Local Geology

In the case of the Karthala massif, the geology of the area is divided into three (03) volcanic units according to the presence or absence of surface flow structures. These lithological units are the following:

- The first unit corresponds to the ancient Karthala (K5 and K6), which is highly altered and does not have surface flow structures and develops layers of ferralitic alterites of decimetric to metric thickness. It is located mainly in the Badjini massif and on the eastern flank;
- a second unit characterized by little altered formations constituting the recent Karthala (K4a and K4b) consisting of pahoehoe and aa type flows, aphyric basalts and mega olivine crystals. It represents the majority of the

volcanic edifice of the sector.

- A third unit is composed of younger formations constituting the current Karthala (K1, K2 and K3) devoid of vegetation with well preserved surface features of the flows. This unit represents the flows of the 19th and 20th centuries.

The Bangaani sector (**Figure 4**) in the Karthala massif is subdivided into three (03) basaltic volcanic formations [3]:

- aa and pahoehoe type flows, aphyric to subaphyric basalts emitted during 1858, 1859, 1862 and 1872 respectively, olivine mega crystal basalts emitted during 1848, 1857, 1858 and 1859, olivine and pyroxene basalts emitted from 1857, 1872 and 1876 or olivine and pyroxene basalts accompanied by rare plagioclases emitted in 1880 [3]. It is named K2.
- flows that are petrographically identical to those of unit K2. Their date of emission is not known. The rocks show no alteration [3]. It is named K3.
- and aphyric basalt flows associated with pyroclastic sheets from magmatic explosions (lapillis and scoriaceous bombs), phreatic or phreatomagmatic. It is called K4a [3].

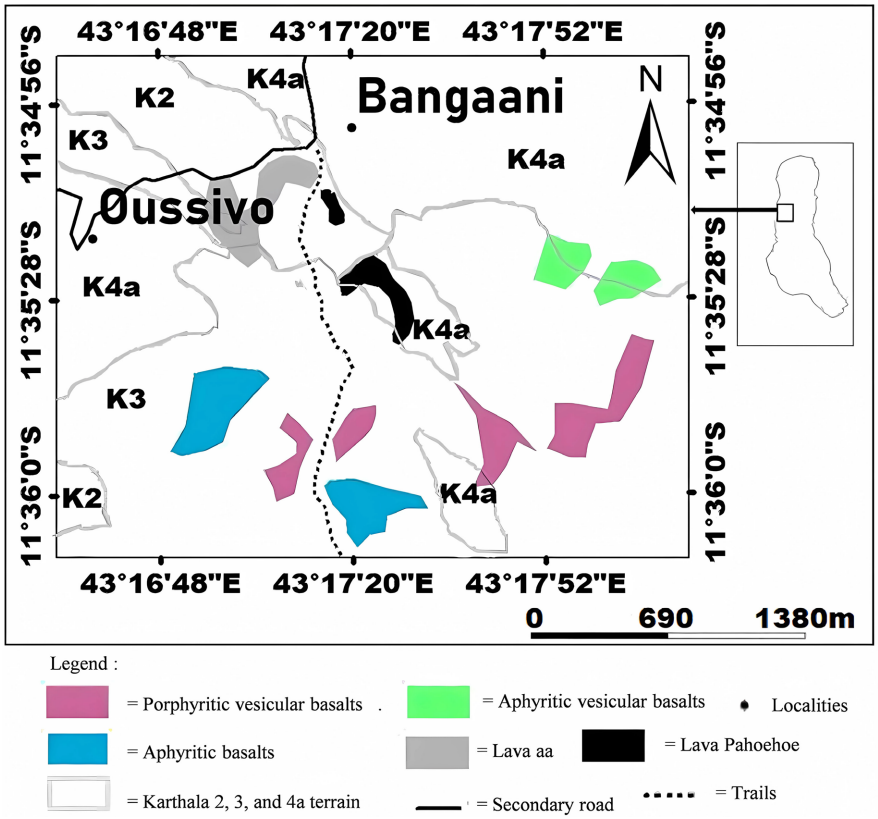

Figure 4. Location of facies studied in the recent (K1 and K3) and present (K4a) Karthala, (Extract from the volcano-tectonic map of Grande Comore) [3], modified. **K2** = Karthala 2; **K3** = Karthala 3; **K4a** = Karthala 4a; **K2** and **K3** = present-day Karthala composed of aphyric non-vesicular basalts, porphyric or aphyric vesicular basalts, and aa and pahoehoe lavas; **K4a** = recent Karthala composed of porphyric or aphyric vesicular basalts and pahoehoe lava.

4. Methodology

The methodology used consists of 1) field work based on the description and systematic sampling of the different volcanic facies outcropping in the Bangaani area, 2) laboratory work consisting of the preparation of thin sections in the geotechnical laboratory of the Institute of Earth Sciences of the Cheikh Anta Diop University of Dakar (UCAD) and petrographic analysis of the samples collected in the Department of Geology of the Dakar University 3) and processing of the geochemical data extracted from the article of [7] and obtained by the ICP-AES method in Clermont-Ferrand.

5. Results

5.1. Lithology

The lithological results (**Figure 4**) obtained from the systematic sampling carried out in the Bangaani sector during the field campaign from October 02 to November 29, 2019, allowed us to locate the studied facies on an extract of the volcano-tectonic map (**Figure 4**) of Grande Comore [3].

In this map, the first unit is that of aa and pahoehoe type flows, porphyritic vesicular basalts, aphyritic vesicular basalts and aphyritic basalts, it represents the present Karthala (K2 and K3). The second unit consists of aa and pahoehoe type flows, porphyritic vesicular basalts and aphyritic vesicular basalts, it represents the recent Karthala (K4).

Lithological and volcanological characteristics allow us to distinguish three (3) types of lava flows in the Bangaani area:

- pahoehoe type lava flows or corded lava flows with smooth undulating or twisted surface (**Figure 5(A)**). They are poor in silica and emitted at very high temperatures. They are very fluid and fast moving,
- aa lava flows with a rough, jagged and generally cleaved surface (**Figure 5(B)**). They are relatively rich in silica, which gives them a high viscosity,
- and porphyritic to aphyritic vesicular massive basalt flows (**Figure 5(C)** and **Figure 5(D)**) and aphyritic non-vesicular basalts (**Figure 5(E)**).

Occasionally, lava tunnels more than 2.5 m long and 4 m wide are observed between aa-type lavas representing the roof and pahoehoe-type lavas representing the wall (**Figure 6**) with a tunnel ceiling bearing basalt stalactites.

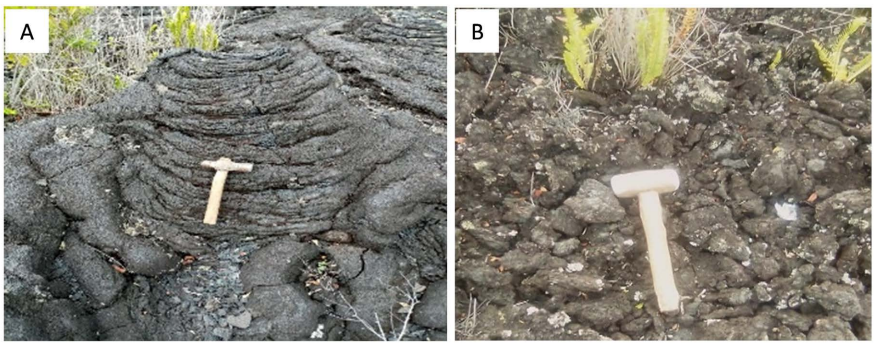

Figure 5. Lava flows in the Bangaani area. **Legend:** A = pahoehoe type flow; B = aa type flow; C = porphyritic vesicular basalt flow; D = aphyritic vesicular basalt flow; E = aphyritic basalt flow.

Figure 6. Lava tunnel between **aa** and **pahoehoe** flows.

Conclusion

The Bangaani sector is essentially characterized by three (3) types of flows: pahoehoe type flows, aa type flows and massive vesicular porphyritic or aphyritic non vesicular basalt flows.

5.2. Petrography

This study focuses on samples of vesicular or nonvesicular basalts taken from massive basalt lava flows outcropping in the Bangaani area.

5.2.1. Porphyritic Vesicular Basalt

The rock reveals a porphyritic microlitic texture composed of plagioclase, clinopyroxene, olivine, and opaque minerals in a relatively abundant mesostasis (**Figure 7(A)** and **Figure 7(B)**).

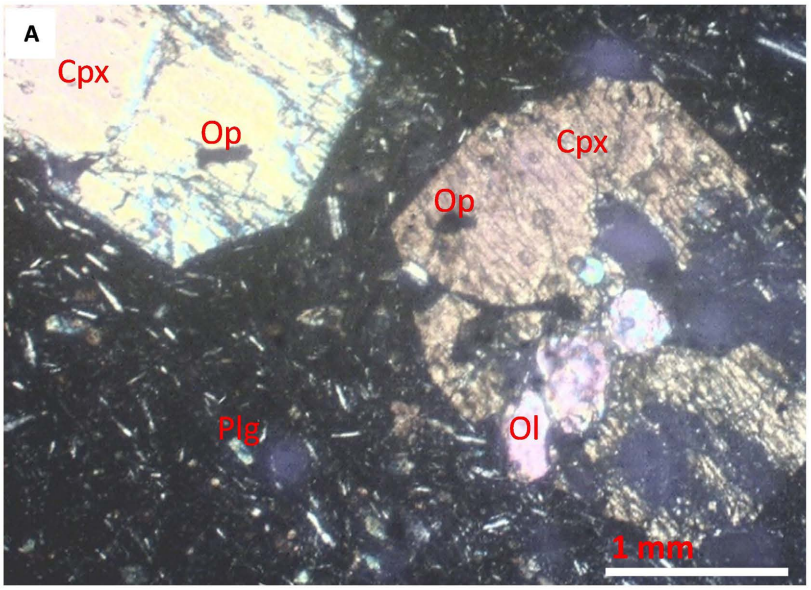

A = Porphyritic microlitic texture showing clinopyroxene phenocrysts containing olivine and opaque mineral inclusions, plagioclase microlites and relatively abundant mesostasis

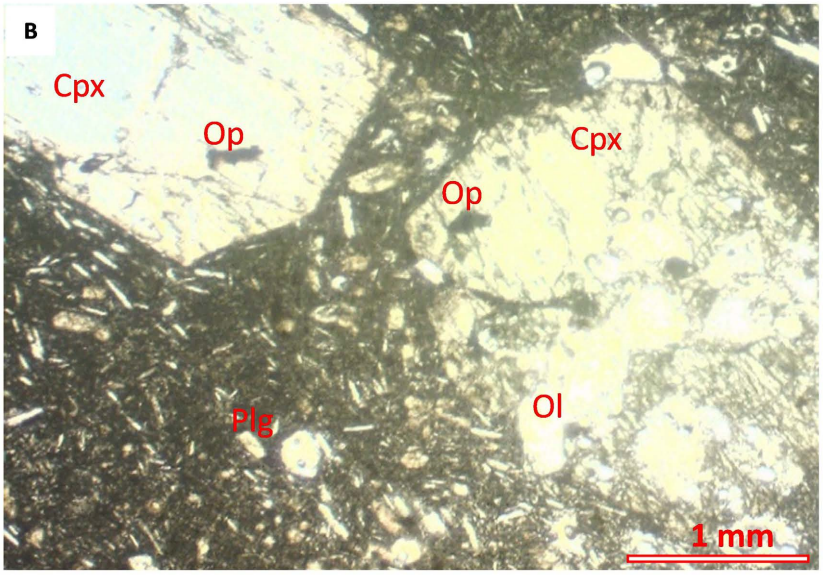

Same texture in LN

Figure 7. LP to LN microphotographs of a vesicular porphyry basalt. **Legend:** Cpx = Clinopyroxene; Plg = Plagioclase; Ol = Olivine; Op = Opaque minerals.

Plagioclases (50% to 55%) occur as numerous microlites in a relatively abundant mesostasis.

Clinopyroxenes (26% to 37%) are in the form of phenocrysts (2.5 - 3.5 mm) or automorphic to subautomorphic microphenocrysts often with a single cleavage direction. Some individuals contain microphenocrysts of olivine and opaque minerals (**Figure 7(A)**).

Olivines (4% to 6%) appear as automorphic to sub-automorphic microphenocrysts (0.4 - 0.7 mm) embedded in clinopyroxenes.

Opaque minerals (1% to 2%) are automorphic (0.1 - 0.45 mm) to xenomorphic microphenocrysts embedded in clinopyroxene phenocrysts.

The relatively abundant mesostasis is rich in plagioclase microlites and consists of clinopyroxene phenocrysts containing inclusions of olivine micrphenocrysts and opaque minerals.

The crystallization order is Ol - Op - Cpx - Plg.

The rock is a porphyritic vesicular basalt with olivine.

5.2.2. Porphyritic Basalt

The rock shows a porphyritic microlitic texture consisting of plagioclase, clinopyroxene, olivine and opaque minerals in a relatively abundant mesostasis (**Figure 8(A)**).

Plagioclases (50% - 56%) occur as numerous microlites in the mesostasis.

Clinopyroxenes (30% to 37%) generally in the form of automorphic (0.1 - 0.6 mm) to subautomorphic microphenocrysts are disseminated in the mesostasis.

The olivines in automorphic phenocrysts (0.5 - 1.4 mm), occupy (2% to 4%) of the total volume of the rock.

Opaque minerals (0.1% to 3%) in the form of small automorphic to subautomorphic crystals (0.1 - 0. 32 mm) are dispersed in a relatively abundant mesostasis.

The mesostasis is relatively abundant. It consists of numerous plagioclase microlites, olivine phenocrysts, plagioclase microlites and opaque minerals.

The crystallization order is: Ol - Cpx - Op- Plg.

The rock is a porphyritic basalt with olivine.

5.2.3. Aphyric Basalt

The rock has a microlitic texture consisting of plagioclase, clinopyroxene, olivine and opaque minerals in a relatively abundant mesostasis (**Figure 8(B)**).

Plagioclase (60% - 66%) occurs as numerous microlites in a relatively abundant mesostasis.

Clinopyroxenes in microphenocrysts (0.35 - 0.65 mm) automorphic to subautomorphic occupy 25% to 31% of the total volume of the rock.

Olivines (1% to 3%) generally in microphenocrysts (0.5 - 1 mm) automorphic to subautomorphic, form a polycrystalline aggregate in the mesostasis.

The mesostasis is relatively abundant and is rich in micrphenocrysts and microlites of plagioclase, microphenocrysts of clinopyroxene and microphenocrysts of olivine.

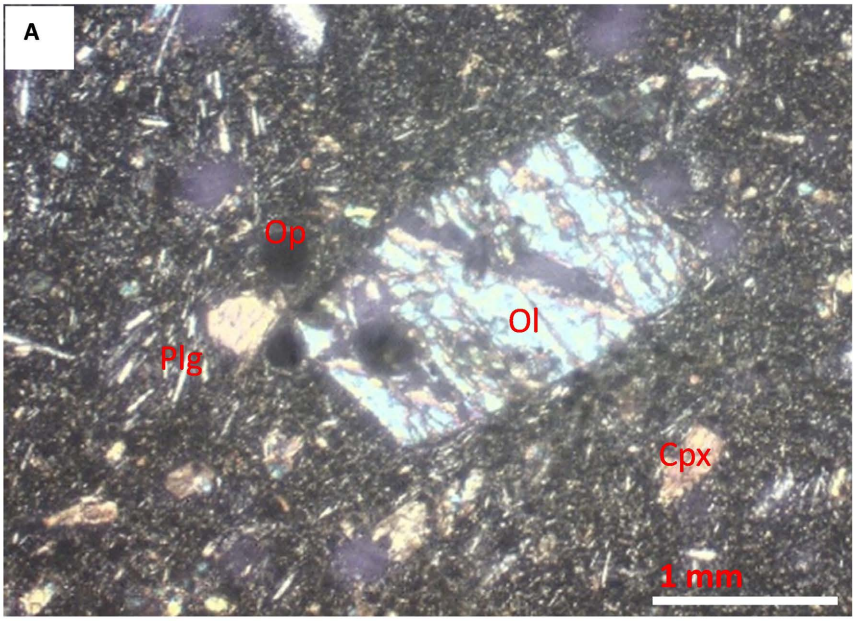

A = Porphyritic microlitic texture in LP showing olivine phenocryst, clinopyroxene microphenocrysts, plagioclase microlites, opaque minerals and relatively abundant mesostasis.

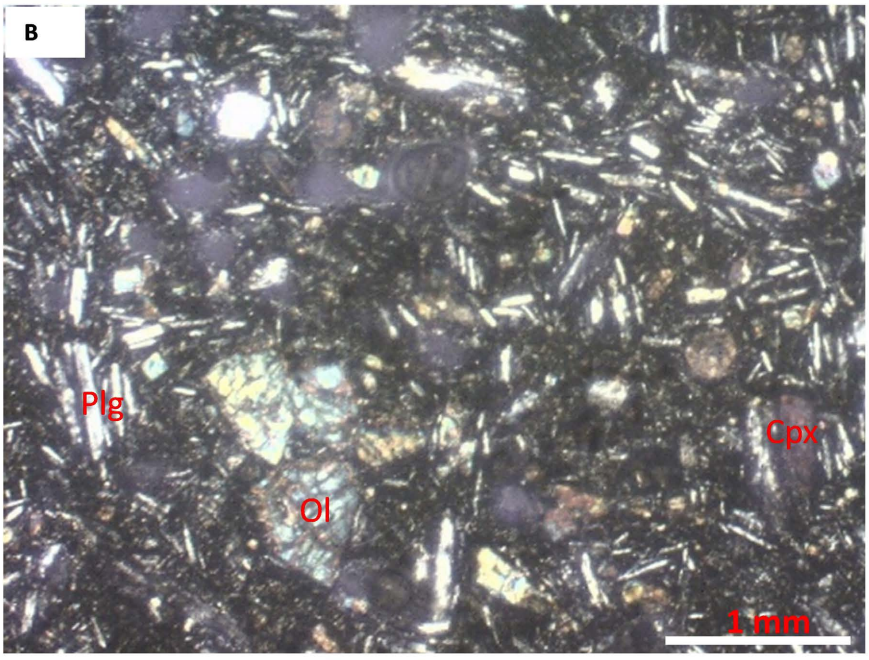

B = Porphyritic microlitic texture in LP showing olivine and clinopyroxene microphenocrysts, plagioclase microlites and opaque minerals

Figure 8. LP microphotographs of a porphyritic (A) and aphyritic (B) basalt. **Legend:** Cpx = Clinopyroxene; Plg = Plagioclase; Ol = Olivine; Op = Opaque minerals.

The crystallization order is: Ol - Cpx - Plg.

The rock is an aphyric basalt.

Conclusion

The microlitic porphyry texture marked by the successive crystallization of

olivines, opaque minerals, clinopyroxenes, and plagioclases in a relatively abundant mesostasis, characterized Karthala the massif basaltic lavas in the Bangaani sector.

This crystallization sequence is typical of a high-pressure environment corresponding to primary alkaline magmas. It shows a slight difference with the Azores OIBs, marked by olivine crystallization followed by clinopyroxene, plagioclase laths, and opaque minerals [11]. However, it differs from the MORBs by the crystallization of plagioclase followed by olivine and clinopyroxene [12], typical of a low-pressure environment.

5.3. Geochemistry

The geochemical study concerns the characterization of the basalts of ancient and recent Karthala. The geochemical data obtained by the ICP-AES method in Clermont-Ferrand [13], are taken from the article of [7]. The results of the different analyses relating to the ancient and recent Karthala are reported in **Tables 1-3**.

Table 1. Geochemical analyses of major, trace and REE elements from old and recent Karthala basalts [7].

	Old KARTHALA						RECENT KARTHALA						
Samples	**87KA3**	**88KA6**	**89KA6Tr**	**89KA8**	**89KA9**	**85KA23**	**85KA34**	**88KA11**	**89KA2**	**89KA3**	**89KA4**	**89KA5**	**89KA7**
Name	**Ba**	**Ba**	**Ba**	**Ba**	**Ba**	**Ba**	**Ba**	**Ba**	**Ba**	**Ba**	**Ba**	**Tr Ba**	**Tr Ba**
SiO_2	48.52	47.4	47.39	48.55	46.30	47.1	47.23	47.28	47.12	45.98	46.72	46.71	47.93
AL_2O_3	14.83	15.33	16.13	12.56	12.80	14.17	14.25	13.23	14.21	11.18	13.61	14.73	14.99
Fe_2O_3	13.41	12.62	12.83	13.15	13.71	13.47	13.45	12.42	13.44	13.03	12.66	13.52	13.17
Mg0	5.51	5.9	5.93	7.20	7.40	6.49	5.38	6.95	5.83	13.56	6.80	5.07	5.06
CaO	10.58	10.81	8.82	12.03	11.29	12.44	10.91	12.72	11.63	10.10	12.74	10.62	10.25
Na_2O	3.19	3.51	3.59	2.56	3.32	3.04	3.57	2.96	3.35	2.57	3.14	3.19	3.7
K_2O	0.9	1.49	2.02	0.89	1.52	1.12	1.44	1.16	1.29	1.01	1.17	1.69	1.51
TiO_2	2.47	2.97	2.73	2.50	2.88	2.52	2.92	2.53	2.67	2.02	2.48	3.13	2.82
MnO	0.17	0.18	0.2	0.18	0.19	0.19	0.19	0.18	0.19	0.18	0.19	0.19	0.19
P_2O_5	0.34	0.53	0.77	0.34	0.54	0.41	0.52	0.42	0.45	0.33	0.45	0.5	0.49
LOI	0.04	0.00	0.22	0.00	0.00	0.00	0.00	0.00	0.00	0.00	0.00	0.00	0.00
H_2O	0.16	0.00	0.32	0.49	0.29	0.00	0.00	0.00	0.00	0.01	0.05	0.00	0.00
Total	99.92	100.74	100.41	99.96	99.95	100.95	99.82	99.85	100.18	99.34	99.96	99.85	100.11
Mg#	44.38	47.59	47.30	51.54	51.18	49.05	44.43	52.78	46.44	66.90	51.12	42.81	43.41
Ni	113	47	72	173	116	100	61	98	62	377	101	43	35
Cr	97	72	124	321	224	159	50	226	32	466	150	28	17
Co	49	52	52	51	56	55	53	55	52	59	52	54	50
Sc	26	29	21	33	26	29	24	35	27	28	32	21	22
Ba	287	575	859	261	436	370	442	390	382	301	380	501	441

Continued

Rb	17	37	51	21	36	26	37	30	32	26	31	41	38
Sr	447	790	1200	421	597	558	574	547	540	417	520	600	571
Y	32	31	35	27	32	28	32	29	29	22	28	32	31
Zr	172	201	361	179	256	170	223	184	189	148	170	220	216
Nb	26	46	83	30	46	39	51	42	45	35	43	53	51
Pb				2.2						2.7			
Th	2.28	3.70	5.73	2.48	4.44	3.75	5.28	4.30	4.25	3.30	4.29	5.14	5.63
U	0.38	0.91	1.58	0.36	0.92	0.87	1.29	0.8	1.04	0.8	1.02	1.26	1.26
La		51		30.4	52.1	44.7		47.9	46.3	36.4	46.8	58.5	
Ce		88.1		56.5	89.4	73		79.3	80.9	61.7	76.8	96.2	
Nd		37.6		27.3	39.3	32.2		33.7	35.8	27.6	33.33	39.4	
Sm		7.18		5.85	7.68	6.54		7.09	6.47	5.24	6.63	8.02	
Eu		2.47		2.08	2.47	2.21		2.2	2.13	1.71	2.15	2.52	
Gd		7.25		6.12	7.3	6.52		6.61	6.46	5.26	6.36	7.51	
Dy		5.76		4.85	5.78	5.18		5.13	5.22	4.13	5.22	5.84	
Er		2.7		2.3	2.81	2.61		2.51	2.67	2.06	2.55	2.98	
Yb		2.23		1.81	2.22	2.06		2	2.08	1.63	2.1	2.38	
Lu		0.3		0.25	0.3	0.27		0.27	0.26	0.21	0.27	0.31	

Legend: Ka = Karthala; Ba = basalt; Tr Ba = Trachy-basalt.

Table 2. Isotopic analyses of old and recent Karthala basalts [7].

Sample	$^{87}Sr/^{86}Sr$	$^{143}Nd/^{144}Nd$	$^{206}Pbr/^{204}Pb$	$^{207}Pb/^{204}Pb$	$^{208}Pb/^{204}Pb$
			Old Karthala		
87KA3	0.70335	0.51278	19.641	15.603	39.522
88KA6	0.70350	0.51272	19.533	15.557	39.425
89KA6	0.70352	0.51278	19.522	15.573	39.488
89KA8	0.70330	0.51282	19.471	15.560	39.480
89KA9	0.70354	0.51273	19.863	15.603	39.643
			Recent Karthala		
85KA23	0.70381	0.51268	19.574	15.571	39.576
85KA34	0.70386	0.51267	19.439	15.569	39.494
88KA11	0.70396	0.51265	19.297	15.543	39.392
89KA2	0.70387	0.51267	19.388	15.552	39.448
89KA3	0.70389	0.51266	19.394	15.558	39.476
89KA4	0.70362	0.51272	19.429	15.570	39.402
89KA5	0.70384	0.51269	19.447	15.538	39.399
89KA7	0.70385	0.51267	19.429	15.559	15.559

Table 3. Rare earth composition of the basalts of the recent and old Karthala, normalized to the C1 chondrites of [22].

	Old Karthala				Recent Karthala					
	88KA6	89KA8	89KA9	89KA9	89KA11	89KA2	89KA3	89KA4	89KA5	C1
La	201.58	120.16	205.93	176.68	189.33	183.00	143.87	184.98	231.23	0.253
Ce	136.59	87.60	138.60	113.18	122.95	125.43	95.66	119.07	149.15	0.645
Nd	78.99	57.35	82.56	67.65	70.80	75.21	57.98	69.96	82.77	0.476
Sm	46.62	37.99	49.87	42.47	46.04	42.01	34.03	43.05	52.08	0.154
Eu	42.08	35.43	42.08	37.65	37.48	36.29	29.13	36.63	42.93	0.0587
Gd	35.54	30.00	35.78	31.96	32.40	31.67	25.78	31.18	36.81	0.204
Dy	22.82	19.25	22.94	20.56	20.36	20.71	16.39	20.71	29.80	0.252
Er	16.27	13.86	16.93	15.72	15.12	16.08	12.41	15.36	17.95	0.166
Yb	13.27	10.77	13.21	12.26	11.90	12.38	9.70	12.50	14.17	0.168
Lu	11.86	9.88	11.86	10.67	10.67	10.28	8.30	10.67	12.25	0.0253
Total	605.62	422.29	619.77	528.79	557.05	553.06	433.26	544.11	669.14	
(La/Yb)N	15.19	11.15	15.58	14.41	15.90	14.78	14.83	14.80	16.32	
(La/Sm)N	4.32	3.16	4.13	4.16	4.11	4.36	4.23	4.30	4.44	
Sm/Yb	3.51	3.53	3.77	3.46	3.87	3.39	3.51	3.44	3.68	
(Gd/YbN	2.68	2.71	2.71	2.61	2.72	2.56	2.66	2.49	2.60	
(La/Nd)N	2.55	2.10	2.49	2.61	2.67	2.43	2.48	2.64	2.79	
(Sm/GdN	1.31	1.27	1.39	1.56	1.42	1.33	1.32	1.38	1.41	
(Dy/Lu)N	1.92	1.95	1.93	1.93	1.91	2.02	1.97	1.94	2.43	
(Gd/LuN	2.99	3.03	3.01	2.99	3	3	3.1	2.92	3	

5.3.1. Loss on Ignition

The loss on ignition measured in the Karthala basalts is 0 except for 2 samples (87KA3 and 89KA6) from the ancient Karthala which have loss on ignition (LOI) values of 0.04 and 0.22 respectively.

5.3.2. Evolution of Major and Trace Elements as a Function of Mg#

The Mg# index considered as an index of magmatic differentiation, was calculated from this formula: Mg# = (MgO/40)/((MgO/40) + (FeO/72)) × 100). Total iron (FeOt) was calculated according to [14] in [15]:

$$FeOt = Fe_2O_3t/1.11$$

The values obtained are reported in **Table 1**.

In the basalts of recent Karthala, the values of Mg# are between 42.81 and 66.90% with an average of 49.61% and between 44.38 and 51.54% with an average of 48.39% in those of ancient Karthala. The relatively high values of Mg# in the basalts of recent Karthala attest to their primitive character compared to the basalts of ancient Karthala, which present slightly more evolved terms.

5.3.3. Major Elements

The diagrams of variations of the main oxides according to the magmatic differentiation index Mg# highlight characteristic trends (**Figure 9**).

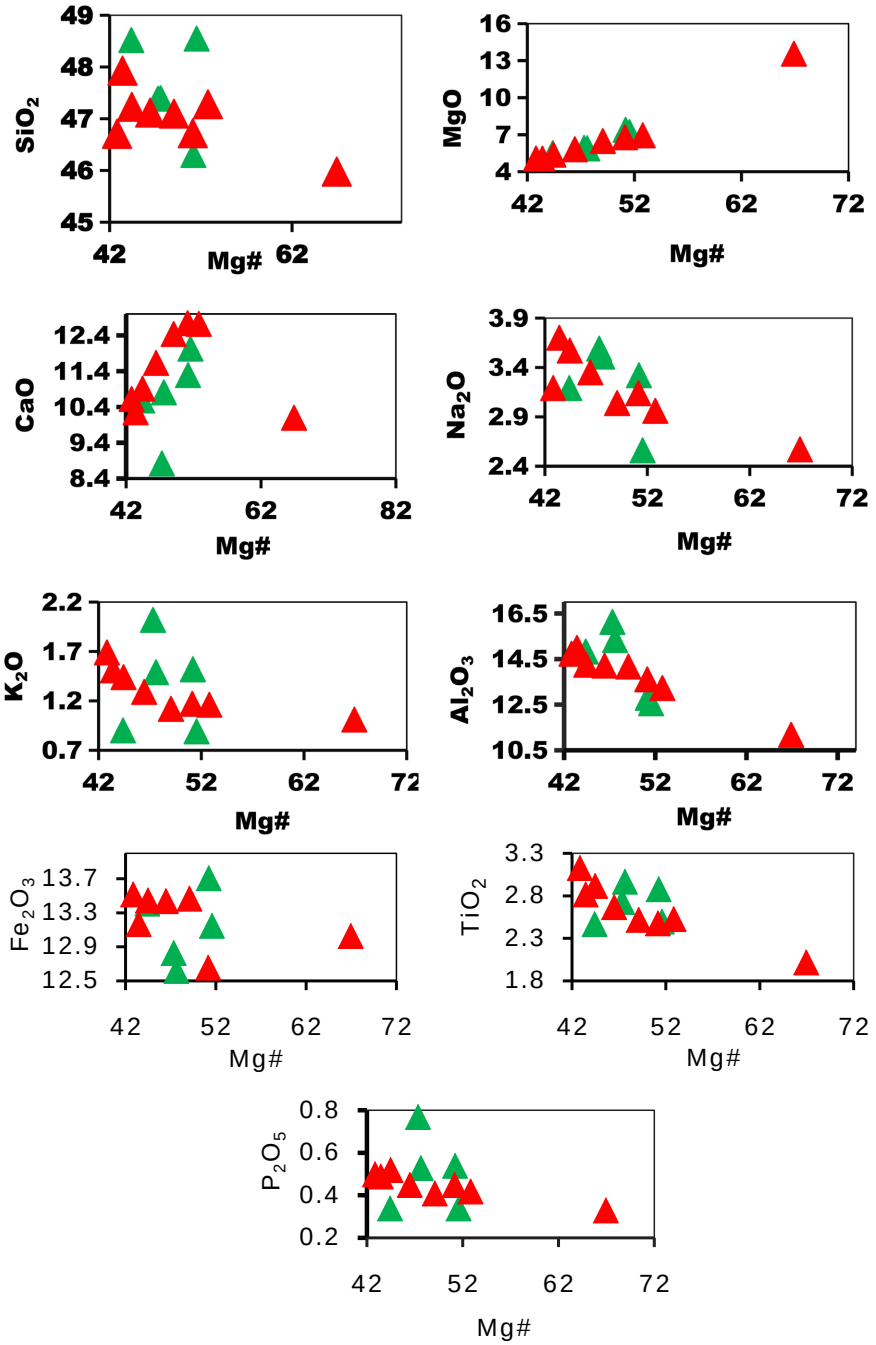

Figure 9. Chemical evolution of major elements as a function of Mg#, Red = Recent Karthala; Green = Old Karthala.

Magnesium and calcium show a good positive correlation with the magmatic differentiation index Mg# despite the low dispersive character of calcium. The behavior of magnesium and calcium shows the importance of clinopyroxene fractionation.

Alkalis show a negative correlation with the magmatic differentiation index although potassium shows slightly more dispersive characters than sodium. This evolution is typical of an alkaline series.

Alumina shows a negative correlation with the magmatic differentiation index Mg# despite the low dispersive character in the ancient Karthala. This evolution may be due to the crystallization of plagioclases.

Titanium shows a negative correlation with the Mg# index. This behavior is in agreement with the fractionation of ferro-titanium oxides.

Silica, iron and manganese show dispersion in the ancient Karthala basalts. The manganese is constant in the basalts of the Recent Karthala. The dispersion of the ancient Karthala samples may be related to lateritic alteration as pointed out by [7].

The low increase in P_2O_5 concentrations reflects the low differentiation of these rocks as well as the absence of apatite fractionation as noted [8].

Conclusion

The study of the evolution of major elements shows a behavior that seems to be in agreement with the crystallization of minerals such as clinopyroxenes, plagioclases and ferrotitanium oxides.

5.3.4. Trace Elements

Their evolution in relation to Mg# is shown in **Figure 10**.

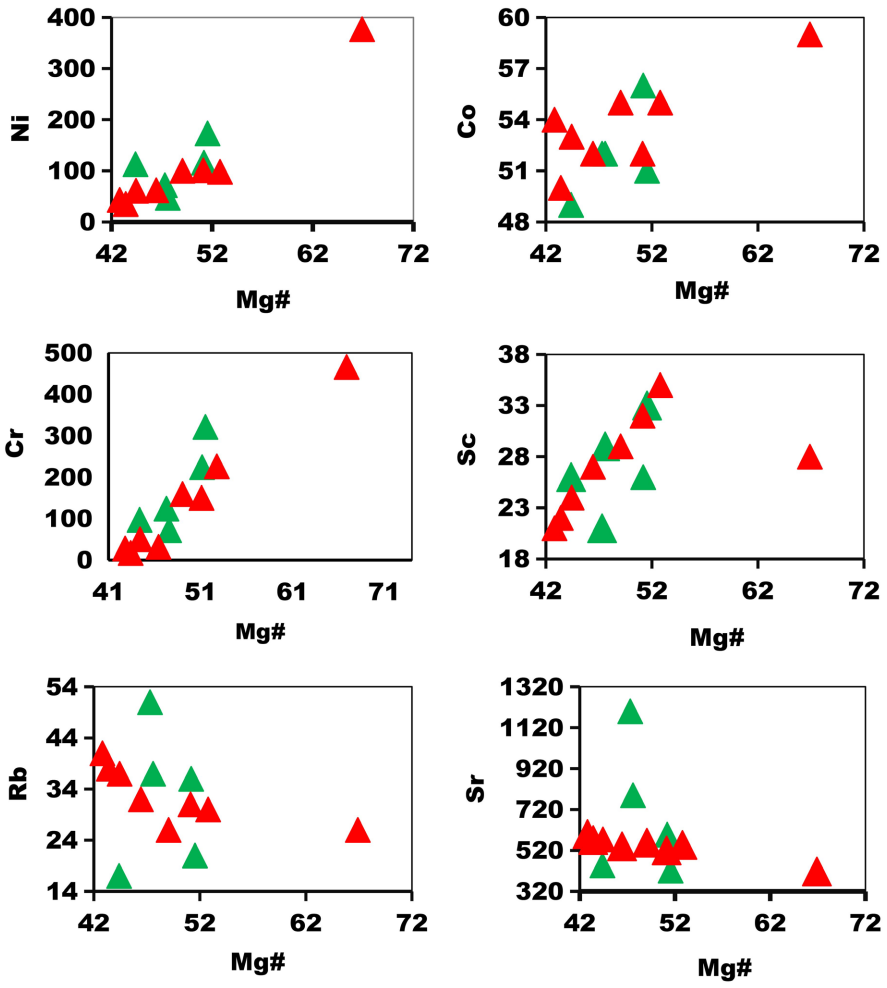

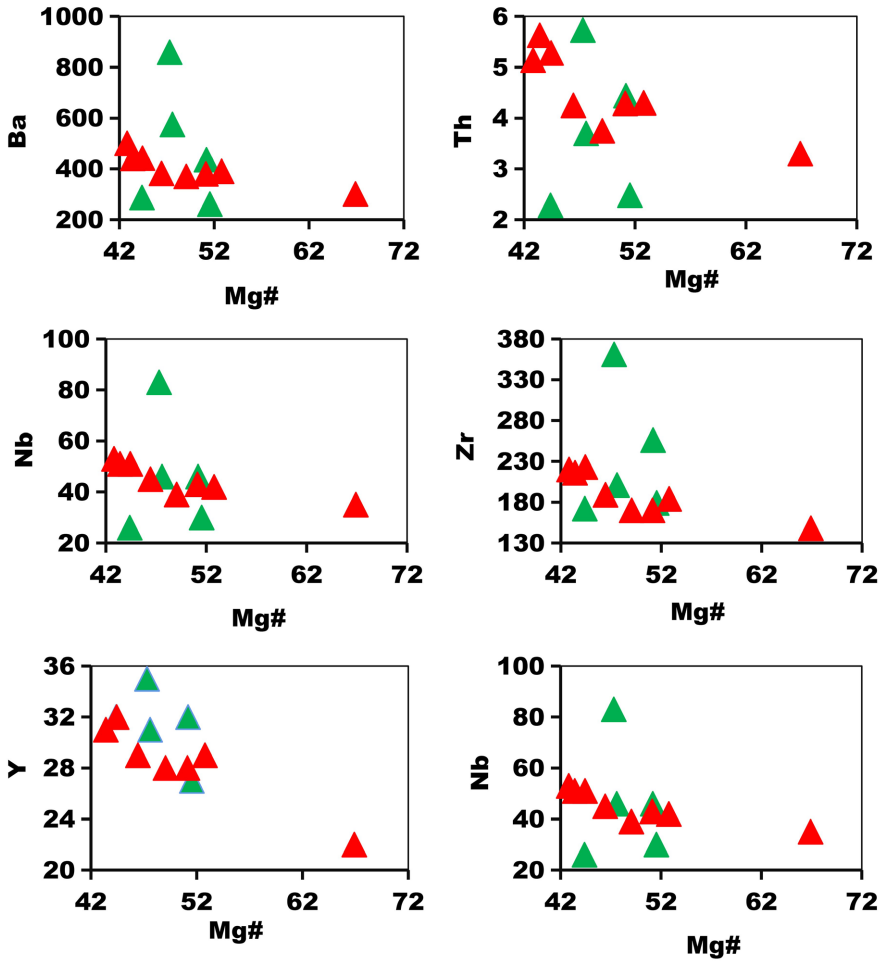

Figure 10. Evolution of trace elements as a function of Mg, Red = Recent Karthala; Green = Old Karthala.

Nickel and cobalt show a good positive correlation with the magmatic differentiation index. The decrease in concentrations of these elements is in agreement with the crystallization of olivines.

Chromium and scandium show a positive correlation with Mg# despite the low dispersive character. This behavior is in agreement with the crystallization of clinopyroxenes.

Strontium, barium and rubidium, which are alkaline elements, show a more or less clear negative correlation with Mg# in the recent Karthala despite the low dispersive character of the ancient Karthala. The behavior of these elements shows the alkaline character of the magma.

Thorium, zirconium, yttrium, niobium and uranium, which are elements known to be hygromagmaphilic, show a weak negative correlation with Mg# in the recent Karthala.

Conclusion

The evolution of trace elements indicates a fractionation of olivine and clinopyroxene then plagioclase.

5.3.5. Nomenclature Diagrams

For the alkaline rocks of recent and ancient Karthala, we have chosen some commonly used nomenclature diagrams. In particular, we use the $Na_2O + K_2O - SiO_2$ diagram of [16] and the Zr/TiO_2 - Nb/Y diagram of [17] modified by [18]. Thus, in the $Na_2O + K_2O - SiO_2$ diagram of [16], almost all of the samples are in the field of basic rocks especially alkaline basalts and trachybasalt. However, two (2) samples from Karthala 87KA3 and 89KA8 are in the calc-alkaline basalt field due to their low alkali content (**Figure 11(A)**). In the Zr/TiO_2 versus Nb/Y classification diagram of [17], modified by [18], all the samples are positioned in the

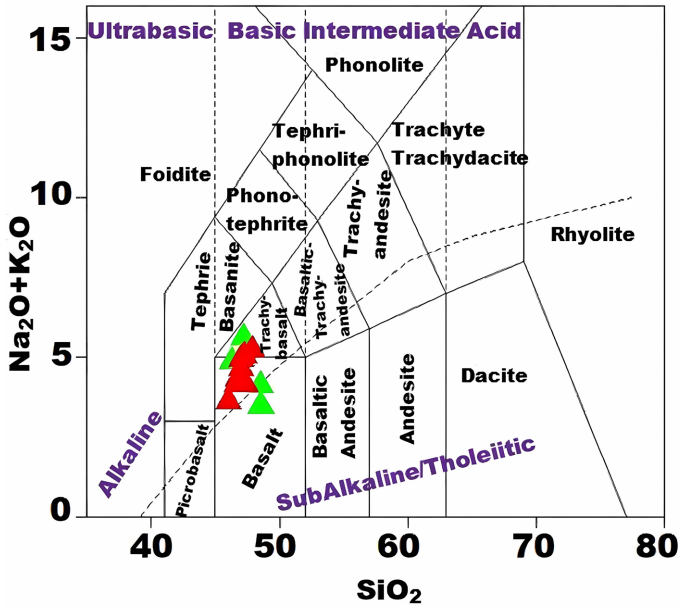

(A)

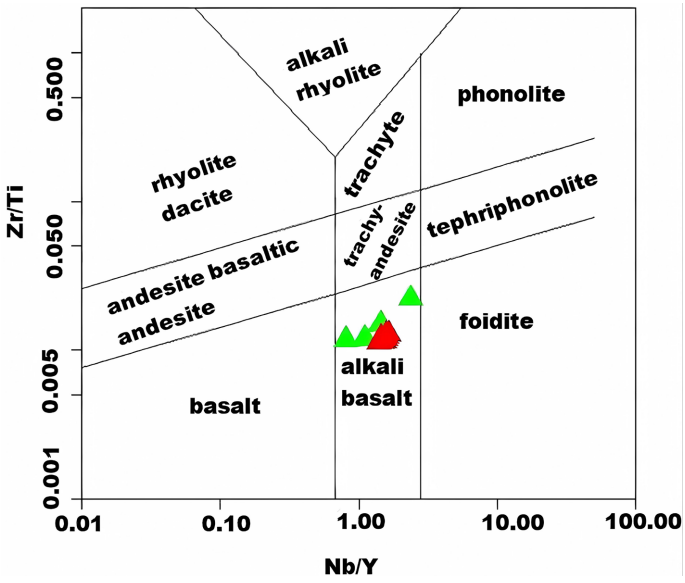

(B)

Figure 11. Position of the Karthala basalts in the volcanic rock diagrams [16], (A) and [17] modified by [18], (B) Red = Recent Karthala; Green = Old Karthala.

alkaline basalt field. This confirms the alkaline character of the Karthala massif basalts (**Figure 11(B)**).

5.3.6. Geodynamic Context Diagrams

In the 2Nb-Zr/4-Y diagram of [19], the samples are positioned in the intraplate basalts (AI) and intraplate alkaline basalts and tholeiths (AII) domain (**Figure 12(A)**). In the diagram of [20], Zr/Y versus Zr, all samples fall into the intraplate

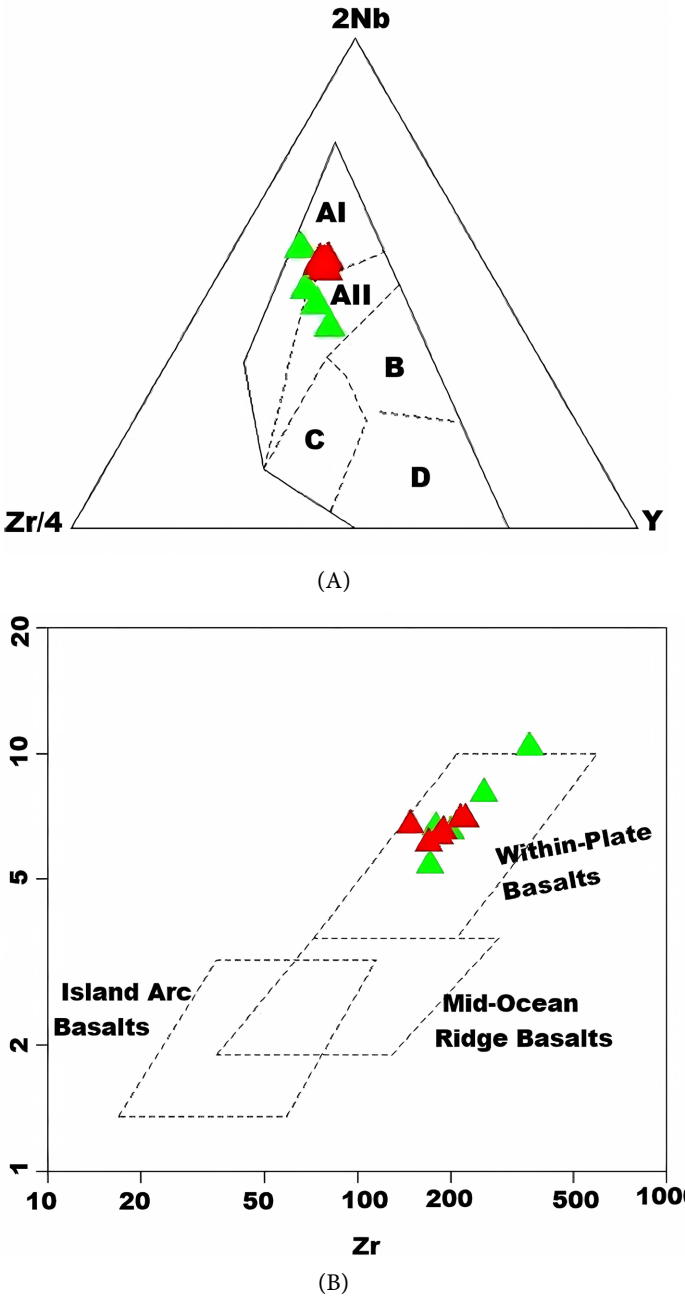

Figure 12. Position of the Karthala basalts in the 2Nb-Zr/4-Y diagram of [19], (A) and Zr/Y-Zr [20], (B). Red = Recent Karthala; Green = Old Karthala. **Legend (A):** AI = Intraplate alkaline basalts; AII = Intraplate alkaline basalts and tholeiths; B = P-MORB basalt; C = Island arc basalts; D = N-MORB and island arc basalts.

basalt domain. This shows that the chemical composition of the basalts of the Karthala massif is compatible with the domain of intraplate basalts. (**Figure 12(B)**).

In the geotectonic discrimination diagram [21] using Th/Yb vs Nb/Yb ratios (**Figure 13(A)**), all the samples studied are positioned in the oceanic domain more specifically in the Oceanic Islands Basalts (OIB) field. In addition, the second diagram [21], TiO_2/Yb vs Nb/Yb (**Figure 13(B)**), all samples are placed

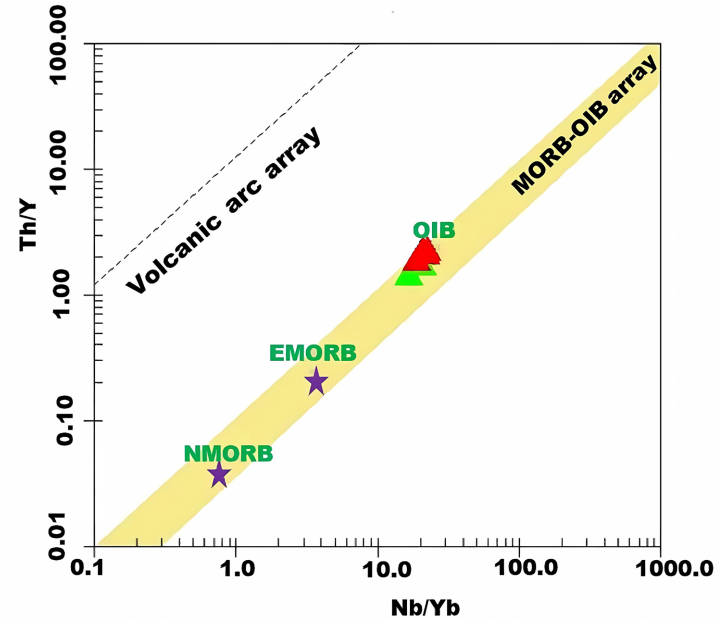

(A)

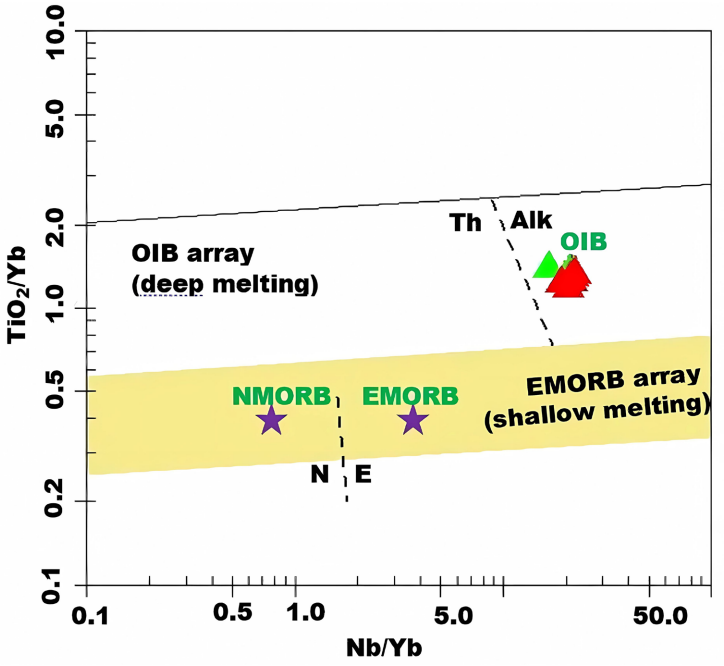

(B)

Figure 13. Position of Karthala basalts in geotectonic discrimination diagrams [21] using Th/Yb vs Nb/Yb (A) and TiO_2/Yb vs. Nb/Yb (B) ratios; Same legend as **Figure 12**.

in the field of alkaline oceanic island basalts (OIB ALk). They have high TiO_2/Yb and Nb/Nb ratios.

5.3.7. Rare Earth Geochemistry

In the diagram normalized to C1 chondrites (**Figure 14**) from [22], the Karthala basalts show steeply sloping spectra (LaN/SmN = 4.13 and LaN/YbN = 14.76) with a subparallel appearance, reflecting an enrichment of LREE (110 to 300 times chondrites) compared to HREE (10 to 20 times chondrites) of the basalts studied.

This enrichment in light rare earths, which are among the most incompatible elements, attests to a low rate of partial melting of the source material at the origin of the Karthala basalts. Furthermore, the spectra at the HREE level can be interpreted as the presence of garnet in the source material implying a greater melting depth.

All these observations allow the basalts studied to be assimilated to alkaline basalts of type OIB (oceanic islands basalts) which are notably enriched in the most incompatible elements but depressed in the least incompatible elements.

The basalts of recent Karthala are more enriched in LREE (LaN/SmN = 4.26 and LaN/YbN = 15.17) than those of ancient Karthala (LaN/SmN = 3.87 and LaN/YbN = 13.96).

5.3.8. Multi-Element Diagram

The multi-element diagram (**Figure 15**) normalized to the primitive mantle [23] shows that the basalts of the Karthala Massif exhibit steeply sloping spectra with a subparallel appearance reflecting enrichment in LILE (Rb, Ba, Th, U, Nb) relative to the HFSE (Zr, Ti,) that is typical of a low partial melt rate of the source material.

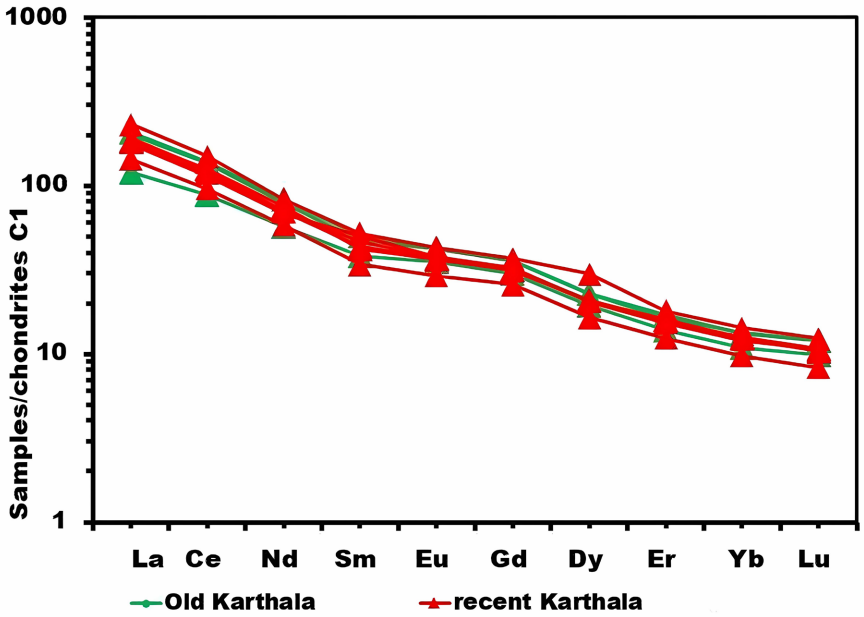

Figure 14. Rare earth spectra normalized to C1 chondrites [21], basalts from recent and old Karthala.

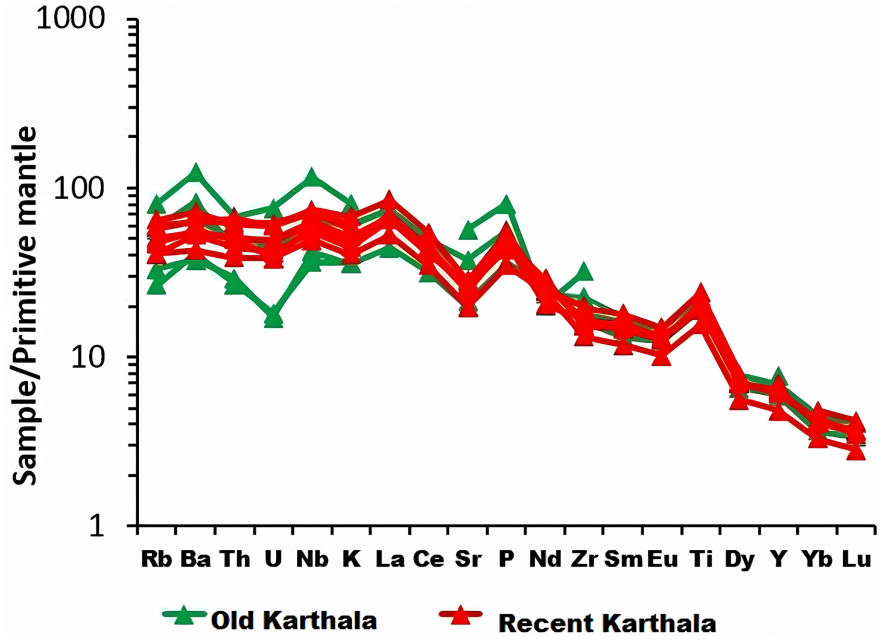

Figure 15. Multi-element trace element diagram normalized to the primitive mantle [23], Karthala basalts, same legend as **Figure 9**.

6. Discussion

The basaltic plateaus of the Bangaani area are characterized by outpourings of pahoehoe or aa basaltic flows and massive basalt flows with different facies. The aa types, which are generally derived from the transformation of pahoehoe, are by far the most widespread in the Karthala massif in contrast to those of the Kilauea volcano in the Hawaiian Islands [24].

The massive basalts of Karthala in the Bangaani area have a microlitic porphyry texture marked by early crystallization of olivine followed by opaque minerals, clinopyroxenes and numerous plagioclase microlites in a relatively abundant mesostasis.

This crystallization sequence is typical of a high pressure environment corresponding to the genesis of alkaline basic magmas. It shows a slight difference with that of the Azores OIBs which are marked by the crystallization of olivines, clinopyroxenes followed by plagioclase laths and opaque minerals [11]. Nevertheless, it differs from that of the MORBs by the early crystallization of plagioclase followed by olivine and clinopyroxene [12], typical of a low pressure geodynamic environment.

The chemical data show an undersaturation in silica and high contents of alkaline elements and titanium. However, the work done by [8] on the Karthala basalts reveals a low degree of undersaturation and a weakly alkaline to transitional character.

The primary character of these basalts marked by relatively high contents of magnesium, nickel, chromium and scandium has been well detailed by [8].

Indeed, the high nickel concentration is related to an assimilation of very nickel-bearing olivine xenocrysts. It could be the consequence of the harvesting

of a variable fraction of olivines particularly rich in nickel by aphyric liquids or having an important fraction of phenocrysts [7].

The Karthala basalts show strongly sloping rare earth spectra with a subparallel appearance (LaN/YbN = 11.15 to 16.31) which reflects an enrichment in LREE (110 to 300 times the chondrites) compared to HREE (10 to 20 times the chondrites) of the basalts studied. The enrichment in light rare earths of the studied basalts is also attested by [7] with LaN/YbN ratios between 12 and 17.6.

Multi-element diagram analysis shows that the Karthala basalts are enriched in incompatible elements (Rb, Ba, Th, U, Nb, LREE) compared to the HFSE and HREE.

The Karthala lavas are essentially the product of a low degree of partial melting. They were emplaced in an intraplate context of OIB type.

In terms of isotope ratios, Karthala lavas have higher $^{87}Sr/^{86}Sr$ values than those of the Cape Verde Peninsula [25] and the Cape Verde Archipelago [26]. The old Karthala lavas are similar to those of St. Helene, which are of type HIMU, whereas those of the recent Karthala are similar to those of Kerguelen, which are of type EM I [27].

7. Conclusions

The Bangaani sector of the Karthala massif is characterized by basaltic plateaus consisting of pahoehoe or aa-type flow spreads and massive basalt flows. The massive basalts have vesicular porphyritic or aphyritic facies and non-vesicular facies that are also porphyritic or aphyritic.

Petrographic analysis of massive basalts is marked by early crystallization of olivine, opaque minerals, clinopyroxene and plagioclase in a relatively abundant mesostasis.

This crystallization sequence is typical of a high pressure environment marked by a low partial melting rate leading to alkaline magmas.

Chemical data in major and trace elements show that the Karthala basalts are alkaline and under saturated in silica. Their relatively high contents of magnesium, nickel, chromium and cobalt attest to their primary character.

Trace element geochemistry allows the basalts studied to be assimilated to alkaline basalts of type OIB by their enrichment in LILE and by their depletion in HREE and HFSE. The depletion in HREE would indicate the presence of garnet in the source material implying a great depth of fusion. In addition, the values of the isotopic ratios allow them to be compared to the HIMU type OIBs from St. Helene and EM I from Kerguelen.

Acknowledgements

We thank the Comoros Geological Survey for material support and assistance during fieldwork (systematic sampling of different volcanic facies).

Our thanks also go to Mr. ABDOU Diouf, head of the geotechnical laboratory of the Institute of Earth Sciences of the University Cheick Anta Diop of Dakar

(UCAD), for the welcome he gave us respectively and for having provided us with all the means to make the thin sections. Thank you for having taught us all the secrets of the realization of thin slides.

Our warm thanks go to Mr. ANLIL Wafa Adaine, Mr. ASNADI Anli, Mr. AYOUBA M'madi and Mr. CHAFIK Bafakih technician at the Volcanological Observatory of Karthala (OVK) who helped us to obtain some bibliographic references.

Conflicts of Interest

The authors declare no conflicts of interest regarding the publication of this paper.

References

[1] Debeuf, D. (2004) Etude de l'évolution volcano-structurale et magmatique de Mayotte (Archipel des Comores, Océan Indien): Approches structurale, pétrographique, géochimique et géochronologique. Thèse, Université de La Réunion, Saint-Denis Cedex, 277.

[2] Hajash, A. and Armstrong, R.L. (1972) Paleomagnetic and Radiometric Evidence for the Age of the Comores Islands, West Central Indian Ocean. *Earth and Planetary Science Letters*, **16**, 231-236. https://doi.org/10.1016/0012-821X(72)90195-1

[3] Bachèlery, P. and Coudray, J. (1993) Notice explicative de la carte volcano-tectonique de la Grande Comore (Ngazidja). Echelle: 1/50,000e, ed. Ministère Français de la Coopération.

[4] Emerick, C.M. and Duncan, R.A. (1982) Age Progressive Volcanism in the Comores Archipelago, Western Indian Ocean and Implications for Somali Plate Tectonics. *Earth and Planetary Science Letters*, **60**, 415-428. https://doi.org/10.1016/0012-821X(82)90077-2

[5] Upton, B.G.J. (1982) Oceanic Islands. In: Nairn, A.E.M. and Stehli, F.G., Eds., *The Oceans Basins and Margins*, Plenum, New. York, 585-648. https://doi.org/10.1007/978-1-4615-8038-6_13

[6] Nougier, J., Cantagrel, J.M. and Karche, J.P. (1986) The Comores Archipelago in the Western Indian Ocean: Volcanology, Geochronology and Geodynamic Setting. *Journal of African Earth Sciences*, **5**, 135-145. https://doi.org/10.1016/0899-5362(86)90003-5

[7] Deniel (1998) Geochemical and Isotopic Sr, Nd, Pb Evidence for Plume-Lithosphere Interactions in the Genesis of Grande Comore Magmas (Indian Ocean). *Chemical Geology*, **144**, 281-303. https://doi.org/10.1016/S0009-2541(97)00139-3

[8] Desgrolard, F. (1996) Pétrologie des laves d'un volcan intraplaque océanique: Le Karthala, île de la Grande-Comore (R.F.I. des Comores). Thèse, Univ. Blaise Pascal, Clermont-Ferrand, 176.

[9] Battistini, R. (1996) Paléogéographie et variété des milieux naturels à Madagascar et dans les voisines: Quelques données de base pour l'étude biogéographique de la (region malgache). Editions de l'orstom, Paris, 1-17.

[10] Malod, J.A., Mougenot, D., Raillard, S. and Maillard, A. (1991) New Constraints on the Kinematics of Madagascar: Tectonic Structures of the Davie Ridge. *Comptes Rendus de l'Académie des Sciences*, **312**, 1639-1646.

[11] White, W.M., Tapia, M.D.M. and Schilling, J.-G. (1979) The Petrology and Geo-

chemistry of the Azores Islands. *Contributions to Mineralogy and Petrology*, **69**, 201-213. https://doi.org/10.1007/BF00372322

[12] Wilson, M. (1989) Igneous Petrogenesis. Department of Earth Sciences, University of Leeds, Leeds. https://doi.org/10.1007/978-1-4020-6788-4

[13] Cantagrel, F. and Pin, C. (1994) Major, Minor and Rare-Earth Element Determinations in 25 Rock Standards by ICP-Atomic Emission Spectrometry. *Geostandards and Geoanalytical Research*, **18**, 123-138. https://doi.org/10.1111/j.1751-908X.1994.tb00511.x

[14] Ragland, P.C. (1989) Basic Analytical Petrology. Oxford University Press, New York, 369.

[15] Sterckx, S. (2018) Géochimie des roches volcaniques archéennes du Groupe de Blake River, ceinture de roches vertes de l'Abitibi, Québec. Université du Québec, Québec.

[16] Le Bas, M.J., Le Maitre, R.W., Streckeisen, A. and Zanettin, B. (1986) A Chemical Classification of Igneous Rocks Based on the Total Alkali-Silica Diagram. *Journal of Petrology*, **27**, 775-750. https://doi.org/10.1093/petrology/27.3.745

[17] Winchester, J.A. and Floyd, P.A. (1977) Geochemical Discrimination of Different Magma Series and Their Differentiation Products Using Immobile Elements. *Chemical Geology*, **20**, 325-343. https://doi.org/10.1016/0009-2541(77)90057-2

[18] Pearce, J.A. (1996) A User's Guide to Basalt Discrimination Diagrams. In: Wyman, D.A., Ed., *Trace Element Geochemistry of Volcanic Rocks*: *Applications for Massive Sulphide Exploration*, Geological Association of Canada Short Course Notes, Vol. 12, St. John's, 79-113.

[19] Meschede, M. (1986) A Method of Discriminating between Different Types of Mid-Ocean Ridge Basalts and Continental Tholeiites with the Nb-Zr-Y Diagram. *Chemical Geology*, **56**, 207-218. https://doi.org/10.1016/0009-2541(86)90004-5

[20] Pearce, J.A. and Norry, M.J. (1979) Petrogenetic Implications of Ti, Zr, Y, and Nb Variations in Volcanic Rocks. *Contributions to Mineralogy and Petrology*, **69**, 33-47. https://doi.org/10.1007/BF00375192

[21] Pearce, J.A. (2008) Geochemical Fingerprinting of Oceanic Basalts with Applications to Ophiolite Classification and the Search for Archean Oceanic Crust. *Lithos*, **100**, 14-48. https://doi.org/10.1016/j.lithos.2007.06.016

[22] Nakamura, N. (1973) Determination of REE, Ba, Fe, Mg, Na and K in Carbonaceous and Ordinary Chondrites. *Geochimica et Cosmochimica Acta*, **38**, 757-775. https://doi.org/10.1016/0016-7037(74)90149-5

[23] Sun, S.S. and McDonough, W.F. (1989) Chemical and Isotopic Systematics of Oceanic Basalts: Implications for Mantle Composition and Processes. *Geological Society*, *London*, *Special Publications*, **42**, 313-345. https://doi.org/10.1144/GSL.SP.1989.042.01.19

[24] Peterson, D.W. and Tilling, R.I. (1980) Transition of Basaltic Lava from Pahoehoe to AA, Kilauea Volcano, Hawaii: Field Observations and Key Factors. *Journal of Volcanology and Geothermal Research*, **7**, 271-293. https://doi.org/10.1016/0377-0273(80)90033-5

[25] Ndiaye, A. and Ngom, P.M. (2008) The Geodynamic Context of the Cenozoic Volcanism of the Cap-Vert Peninsula (Senegal). *International Journal of Geosciences*, **5**, 1521-1539. https://doi.org/10.4236/ijg.2014.512124

[26] Torres, P., Silva, L.C., Munha, J., Caldeira, L., Mata, J. and Tassinari, C. (2010) Petrology and Geochemistry of Lavas from Sal Island: Implications for the Variability

of the Cape Verde Magmatism. *Cominucacoes Geologicas*, **97**, 35-62.

[27] Chauvel, C. and White, W.M. (1998) Géochimie isotopique du volcanisme océanique actuel. Identification des grands domaines mantelliques sources. In: Hagemann and Treuil, Eds., *Introduction à la Géochimie et ses Applications*, CEA, Manson T.1, Chap. 5, 269-286.